Stresses Developed around Displacement Piles Penetration in Sand

Z. X. Yang[1]; R. J. Jardine[2]; B. T. Zhu[3]; and S. Rimoy[4]

Abstract: Establishing the stress conditions developed around displacement piles in sands is crucial to improving the understanding and modeling of their behavior. High-quality experiments and theoretical analyses are providing new insights into the effects of penetration on stress conditions. This paper synthesizes the findings from three independent experimental studies on normally consolidated silica sands and a trio of numerical analyses that tackle the problem from different perspectives. The significant degrees of uncertainty in the measurements and predictions are recognized and significant differences between data sets are discussed and largely resolved. Applying a consistent normalized interpretive framework leads to clear common trends regarding how installation affects the stress regime. While the main emphasis is placed on the radial effective stresses developed around pile shafts, the circumferential and vertical stress states are also considered. **DOI: 10.1061/(ASCE)GT.1943-5606.0001022.** © *2013 American Society of Civil Engineers.*

Author keywords: Displacement pile; Sands; Stress analysis; Stress path.

Downloaded from ascelibrary.org by Zhejiang University on 03/03/15. Copyright ASCE. For personal use only; all rights reserved.

Introduction

The field testing of piles equipped with high-quality surface stress transducers (SSTs) by Lehane et al. (1993) and Chow (1997) revealed that extreme stress changes occur during penetration in sand, especially around the tips. The radial stress, σ'_{rc}, acting against the shafts at any given depth (z) after installation, was shown to vary directly with local cone penetration test (CPT) resistance, q_c, reflecting sand stiffness and state, and reduce systematically as the pile advanced and the relative height above the tip, $h = z - z_{tip}$, increased. A weak dependence on the free-field vertical effective stress, σ'_{zo}, was also identified. Jardine et al. (2005) proposed Eq. (1) for use in the design of cylindrical piles driven in silica sands

$$\sigma'_{rc} = f(z) = 0.029 q_c (\sigma'_{zo}/p_A)^{0.13} (h/R)^{-0.38} \quad (1)$$

where p_A = atmospheric pressure. The q_c and h/R terms have strong influences, while each 10-fold change in σ'_{zo} leads to a change of just 35% in σ'_{rc}. It has been argued that the number of load cycles imposed during installation (White and Lehane 2004) and time effects (Jardine et al. 2006) may also be influential, although these factors are generally neglected in practice. The Imperial College Pile (ICP) design rules, which incorporate Eq. (1), effective stress shaft failure criteria, and new base capacity rules have been validated through comprehensive field test axial capacity database studies that demonstrated no systematic bias and gave a coefficient of variation, <0.30, which is far below the values applied to conventional approaches (Jardine et al. 2005). This approach is now utilized in offshore engineering [Jardine et al. 2005; Overy 2007; American Petroleum Institute (API) 2011] where an equivalent radius R^* is substituted into Eq. (1) for coring open-ended piles, calculated from the pile's outer and inner radii (R_o and R_i) as $R^* = (R_o^2 - R_i^2)^{1/2}$. In the alternative CPT-based approach proposed by Lehane et al. (2005), termed the UWA approach, a scalar reduction factor is applied to σ'_{rc} that depends on the pile geometry and incremental filling ratio (IFR) (Lehane et al. 2005). The UWA and ICP approaches predict that the equivalent average end-bearing resistances, q_b, of plugging tubular piles should decline in relation to q_c as pile diameter D increases, when all other factors are held constant. However, the alternative CPT-based approach proposed by Kolk et al. (2005), termed the Fugro-05 procedure, and that set out by Clausen et al. (2005) in the NGI-05 approach do not anticipate any variation of q_b/q_c with D. In a similar way, the UWA, ICP, and Fugro methods all indicate that local shaft resistance τ_{rzf} should fall (when all other factors are constant) as pile slenderness (L/D) increases, leading to a prediction that local shaft resistance should increase with D when L is held constant. This feature, which has been questioned by Knudsen et al. (2012), is not incorporated into the NGI method. Further discussions on these and other related points are given by Jardine and Chow (2007).

Establishing the full stress field around the piles is crucial to settling the questions raised previously and advancing the understanding and modeling of driven pile soil-structure interaction, load-displacement response, group action, and time-dependent behavior. An accurate numerical analysis has the potential to provide powerful insights. But the extreme stresses, large strains, high degree of nonuniformity, moving boundaries, load cycling, interface shear, particle breakage, and principal stress axis rotation involved all impose modeling difficulties. Most analyses have been limited to highly idealized cavity expansion treatments, which have been found to fit poorly with measurements made around pile shafts in careful experiments (Jardine et al. 2013a, b). More plausible numerical investigations of pile penetration in sand are now feasible

[1]Associate Professor, Key Laboratory of Soft Soils and Geoenvironmental Engineering of Ministry of Education, Research Center of Coastal and Urban Geotechnical Engineering, Dept. of Civil Engineering, Zhejiang Univ., Hangzhou, 310058, China (corresponding author). E-mail: zxyang@zju.edu.cn

[2]Professor, Dept. of Civil and Environmental Engineering, Imperial College, London SW7 2AZ, U.K. E-mail: r.jardine@imperial.ac.uk

[3]Principal Engineer, NOMA Consulting Pty Ltd., 10 Sackville Close, Brisbane, QLD 4018, Australia. E-mail: bitang.zhu@noma-consulting.com

[4]Lecturer, Dept. of Transportation and Geotechnical Engineering, Univ. of Dar es Salaam, Dar es Salaam, Tanzania. E-mail: rimoy@udsm.ac.tz

Note. This manuscript was submitted on January 29, 2013; approved on August 7, 2013; published online on August 16, 2013. Discussion period open until April 27, 2014; separate discussions must be submitted for individual papers. This paper is part of the ***Journal of Geotechnical and Geoenvironmental Engineering***, © ASCE, ISSN 1090-0241/04013027 (13)/$25.00.

through advanced discrete element method (DEM) and FEM techniques. DEM modeling allows particle and interface contact laws to be varied and can cope readily with large deformations and contact changes. Campos et al.'s (2005) DEM analyses examined the stress concentrations and particle movements around pile tips, while Kinloch and O'Sullivan (2007) investigated CPT penetration mechanisms with two-dimensional (2D) analyses. Lau et al. (2010) emphasized the importance of rolling resistance in penetration simulations. Arroyo et al.'s (2011) three-dimensional (3D) DEM CPT modeling was able to show quantitative agreement with tip resistance experiments. Noting that DEM analyses of the surrounding stress field remains limited by the number of particles that can be considered, this paper focuses on assessing the degree to which advanced FEM analyses match the new experimental data. Herein, three independent studies are considered:

- Sheng et al.'s (2005) approach, which applied a Lagrangian multiplier pile-soil contact method to study steady penetration.
- The zipper-type technique employed by Henke and Grabe (2006, 2007), Henke (2008), Grabe and Henke (2010), and Qiu et al. (2011) in which a frictionless rigid pilot tube of very small diameter was used to guide the penetrating pile. A Coulomb friction contact was also simulated between the pile and sand in combination with a coupled Eulerian-Lagrangian (CEL) approach, where the sand mass was discretized with an Eulerian mesh with appropriate element sizes, while both the pile and pile-soil interface were treated with Lagrangian descriptions.
- Zhang et al.'s (2013) arbitrary Lagrangian Eulerian (ALE) finite-element (FE) approach is considered. The latter applied remeshing and variable remapping to simulate monotonic penetration, as well as a constitutive model incorporating breakage mechanics.

Table 1 gives further details of these studies. Zhang et al.'s application of breakage mechanics followed experimental observations by Yang et al. (2010) that particle crushing, shear banding, and interface abrasion processes occurred beneath and around displacement piles in sands that could affect the pile-soil stress regime.

Experimental Studies

Calibration Chamber Experiments

This paper considers measurements made with normally consolidated silica sands in two sets of calibration chamber (CC) experiments and a single centrifuge study, as summarized in Table 1. The experiments may be subject to unintended and possibly neglected influences from instrument calibration characteristics, chamber boundary conditions, pile tip geometry, material and roughness, and grain-scale effects. Further on in the text, the degree to which it is currently possible to measure the stresses consistently around displacement piles in sands will be discussed.

Calibration chambers were introduced to calibrate penetration tests in uniform, well-characterized sands under controlled pressure or displacement boundary conditions. CCs have been adapted for displacement pile studies by Golightly and Nauroy (1990), Foray et al. (1993, 1998), Paik and Salgado (2003), Gavin and Lehane (2003), White and Bolton (2004), Paik et al. (2011), and others. CCs offer better conditions than field tests to measure stresses in the soil mass during installation [starting with Nauroy and Le Tirant (1983) and Foray (1991)] and also to sample the sand after installation. However, analyses by Salgado et al. (1998) and experiments by Rimoy (2013) show the importance of adopting either a large chamber-to-pile diameter ratio (ideally, >100) or an active lateral boundary stress control system (Huang and Hsu 2005) to avoid potential deviations from field behavior. Joint research by Imperial College London and

Table 1. Summary of Key Features of Considered Stress Measurements or Predictions

		Chamber	Sand				Boundary conditions				Pile and installation method			
Reference	Method	internal diameter (mm)	d_{50} (mm)	D_r (%)	D_{pile}/d_{50}	$D_{chamber}/D_{pile}$	Surcharge/ acceleration (kPa)	Lateral boundary	Chamber wall friction	Sensor calibration	Type	D_{pile} (mm)	L_p (mm)	Installation Number of cycles (N)
Jardine et al. (2009, 2013a, b)	CC test	1,200	0.21	72	171	33.3	150–200	Rigid	Minimized by latex membrane	Nonlinear loading-unloading	Closed-ended cone	36	920–1,000	Jacking cycles $N = 50–200$
Allard (1990)	Centrifuge	152	0.1	57.5	95	16.0	50g	Rigid	N/A	Nonlinear loading-unloading	Closed-ended flat	9.5	188	Driving $N_{blow} = 240–300$
Gavin and Lehane (2003)	CC test	1,680	0.22	30 ± 2	518	14.7	40 kPa bottom	Rigid	Reduced by smooth HDPE lining	N/A	Open-ended flat	114	1,600	Jacking cycles $N = 16$
Sheng et al. (2005)	FEM	580	0.32	76	94	19.3	66.7g	Rigid	0	N/A	Closed-ended cone	30	230	Steady pushing $N = 1$
Henke et al. (2010); Qiu et al. (2011)	FEM	10,000	0.16[a]	20, 40, and 75	1,875	33.3	1g	Rigid	0	N/A	Closed-ended cone	300	5,000	Steady pushing $N = 1$
Zhang et al. (2013); I. Einav (personal communication, 2012)	FEM	The axis-symmetric FE model simulating CC tests reported by Jardine et al. (2013a, b)								N/A	Closed-ended cone	36	450	Steady pushing $N = 1$

Note: HDPE = high-density polyethylene.
[a]The $d_{50} = 0.16$ mm of Mai-Liao sand is sourced from Feng et al. (2000) while not specified in Henke et al. (2010) or Qiu et al. (2011).

Downloaded from ascelibrary.org by Zhejiang University on 03/03/15. Copyright ASCE. For personal use only; all rights reserved.

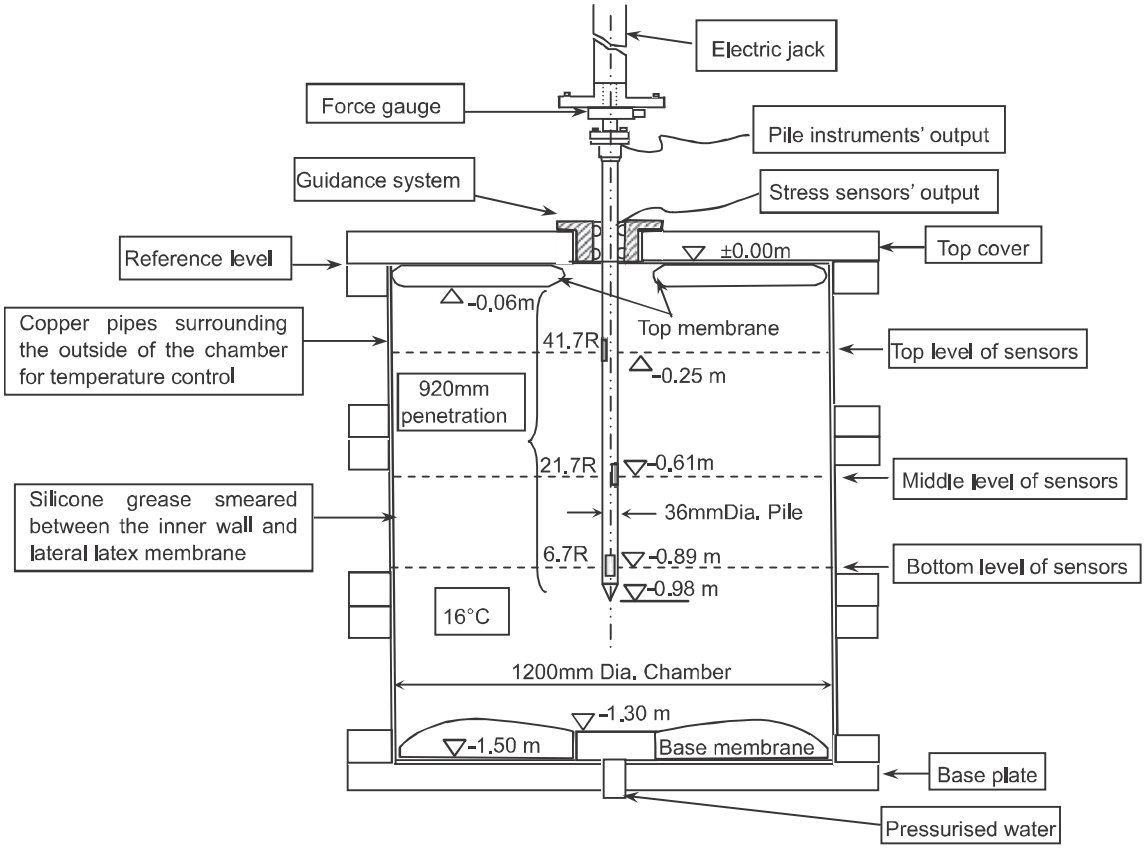


Fig. 1. Schematic of mini-ICP1 test showing one example of instrument layout (Jardine et al. 2009)

INPG (Institut Polytechnique de Grenoble) provides perhaps, the most comprehensive published CC study of the stresses developed around closed-ended displacement piles. Cone-ended mini-ICP stainless steel, moderately rough ($R_{CLA} \approx 3\mu$m) piles with 36-mm outer diameters (OD) were penetrated into dry pressurized, highly instrumented, medium-dense siliceous Fontainebleau NE34 fine sand. Cyclic jacking was employed and typically 50–200 strokes (with full unloading between each) were applied to penetrate ~1 m. Jardine et al. (2009) reported the general experimental arrangements outlined in Fig. 1. The mini-ICP instrumentation included reduced-scale SSTs to measure radial and shear shaft stresses at $r/R = 1$ and three levels on the pile shaft, $h = 6.7R$, $21.7R$, and $41.7R$, respectively. Measurements were also made of σ'_z, σ'_θ, and σ'_r at two to three levels in the sand mass at radial distances between 2 and $20R$ from the pile axis using miniature soil sensors. Zhu et al. (2009) emphasize the highly nonlinear and hysteretic behavior of stress measuring cells and notes that both complex calibration and data reduction procedures are required to obtain reliable data. Two membranes with different central internal diameters (IDs) were used to apply a surcharge pressure of $\sigma'_{zo} \approx 150$ kPa to the sand mass. Separate CPT tests established q_c profiles for various boundary conditions. As shown in Fig. 2, both membrane designs gave quasi-constant CPT trace sections with $q_c = 21 \pm 2$ MPa, although this was achieved at a shallower depth with the smaller ID membrane. Also shown in the figure revised from Jardine et al. (2013b) is the q_c profile predicted independently by Zhang et al. (2013) that is examined comparatively later. Multiple load tests revealed axial capacities that compare encouragingly well with predictions made with the field-calibrated ICP capacity approach. Jardine et al. (2013a, b) report and interpret these experiments, which are referred to here as the mini-ICP dataset and provide the paper's

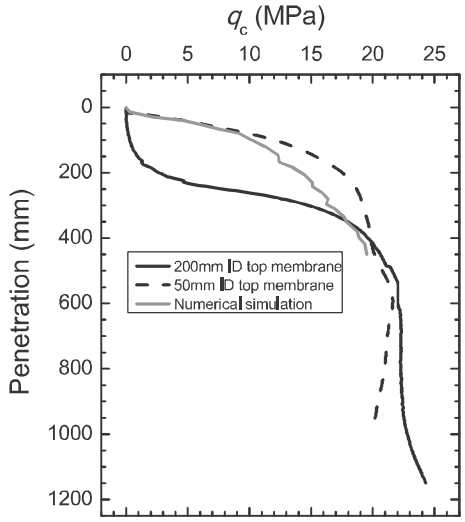


Fig. 2. Cone resistance q_c profiles for alternative top-membrane designs (Jardine et al. 2013b; Zhang et al. 2013)

main experimental benchmark. Rimoy (2013) describes more elaborate experiments with the same equipment.

Gavin and Lehane (2003) report earlier, less extensive, CC stress measurements made around an open-ended relatively smooth ($R_{CLA} \approx 0.4\ \mu$m) stainless steel pile with an external diameter of 114 mm and wall thicknesses of 8.3 mm. The pile was jacked up to 1.6 m and into a 2.3-m-high and 1.68-m-diameter testing chamber filled with dry, uniform, and fine-to-medium siliceous ($d_{50} = 0.22$ mm, $C_u = 1.6$)

Downloaded from ascelibrary.org by Zhejiang University on 03/03/15. Copyright ASCE. For personal use only; all rights reserved.

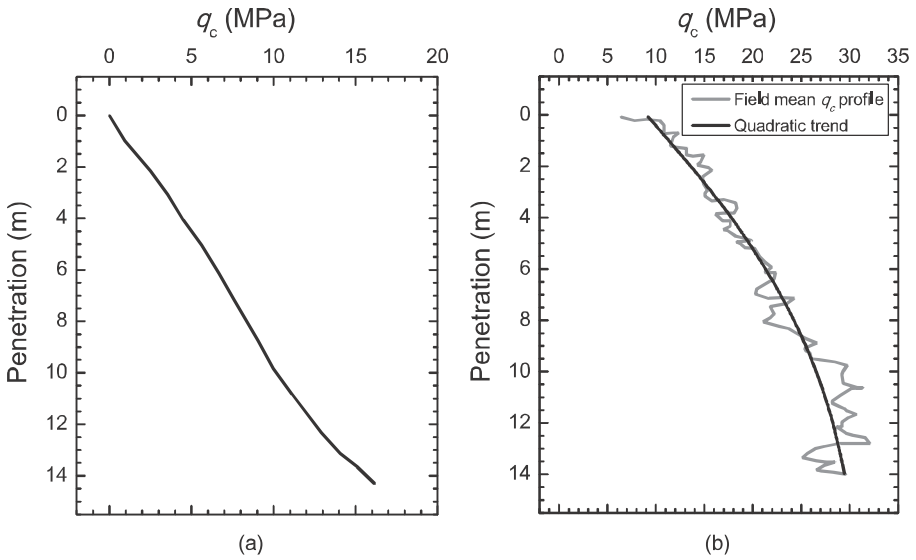


Fig. 3. Typical CPT profiles: (a) LCPC centrifuge test in Fontainebleau sand (Gaudin et al. 2005); (b) field condition in uniform dense sand at Blessington test site (Ireland) (Doherty and Gavin 2010)

sand placed at $D_r = 30 \pm 2\%$; 16 jack strokes were employed. CPT q_c profiles were established independently. The open-ended pile showed coring incremental filling ratios (IFR) close to 100%, down to $z = 0.6$ m, and progressive plugging reduced the IFR to ~14% at the final depth.

Centrifuge Experiments

Centrifuges provide powerful insights into complex problems and help to identify fundamental underlying mechanisms. However, they also call into question potential particle-to-model scale effects, pile roughness issues, stress nonuniformities, and sidewall constraining concerns that may affect any detailed measurements made. The q_c-depth profiles developed in field, calibration chamber, and centrifuge tests also differ. Centrifuge CPT tests generally vary linearly with depth in uniform sands [see Fig. 3(a)], while calibration chamber tests tend to give near parabolic, q_c–σ'_{zo}, relationships (Baldi et al. 1986). Field data appear to resemble the CC trend more closely, as illustrated in Fig. 3(b), which brings together for comparison a field CPT-q_c profile and an interpreted quadratic trend proposed by Doherty and Gavin (2010).

Centrifuge studies involving displacement piles in sand include those by Allard (1990), de Nicola and Randolph (1997), Klotz and Coop (2001), Sakr and Naggar (2003), White and Lehane (2004), and Levacher et al. (2008). Allard (1990) made soil stress measurements in experiments where a smooth 9.5-mm-diameter closed-ended stainless steel pile was driven into a 152-mm-diameter centrifuge bucket filled with dry, uniform Nevada fine silica sand. The fine ($d_{50} = 0.1$ mm) sand was placed at 1,590 kg/m^3 (with $e_0 = 0.65$, $D_r = 57.5\%$). Vertical and radial stresses measured with strain-gauged diaphragm cells (2.6–5.1 mm in diameter) whose strong cell action effects Allard identified and modeled in high-acceleration centrifuge calibration tests. However, the pile driving soil stresses raised to maxima almost double the calibration limits, leading to some measurement uncertainty.

Normalization of Stresses

The experimental and theoretical studies summarized in Table 1 involve a range of pile details (closed and open, rough and smooth), initial effective stress levels (which vary by a factor of > 50 between cases), and boundary conditions and sands with loose-to-dense states. Careful normalization is vital to synthesizing the data and identifying common trends. The experiments all show that the stresses around and below the piles vary sharply with radial distance, r, from the pile axis, as well as relative height above (positive h) or below (negative h) the pile tip. Combining these observations with the field trends encapsulated in Eq. (1) suggests that σ'_z, σ'_θ, and σ'_r can be normalized for variations in local q_c and free-field vertical stress σ'_{zo}, and represented by 2D functions with the form

$$(\sigma'/q_c)\Big/(\sigma'_{zo}/p_A)^{0.13} = f(h/R, r/R) \tag{2}$$

By implication, the equivalent radius R^* should be substituted for R when dealing with predominantly coring open-ended piles, although the functions are likely to differ, especially in the near-field close to the pile shaft where $r/R = 1$. In principle, cyclic and monotonic installation procedures could also produce different functions; time and scale effects could also be significant. This normalization is applied in the interpretation and comparisons given subsequently. Emphasis is placed on the radial effective stresses, but the circumferential and vertical stress states are also considered.

Comparison of Experimental Studies

Benchmark Mini-ICP Set

The benchmark mini-ICP dataset is considered first. Pile penetration invoked extreme stress changes in all three normal stress components, and significant stress changes out to $r/R > 30$. The synthesis of thousands of mini-ICP installation stress measurements led to contour plots for all of the cylindrical stress components including the radial stress set given in Fig. 4 [reproduced from Jardine et al. (2013a)], where the results have been normalized for q_c. No correction is made for $(\sigma'_{zo}/p_A)^{0.13}$ in this plot. However, note that the ratio remained close to unity (1.05–1.06) in these experiments. Fig. 4(a) shows at two scales how the normalized stresses

Downloaded from ascelibrary.org by Zhejiang University on 03/03/15. Copyright ASCE. For personal use only; all rights reserved.

Downloaded from ascelibrary.org by Zhejiang University on 03/03/15. Copyright ASCE. For personal use only; all rights reserved.

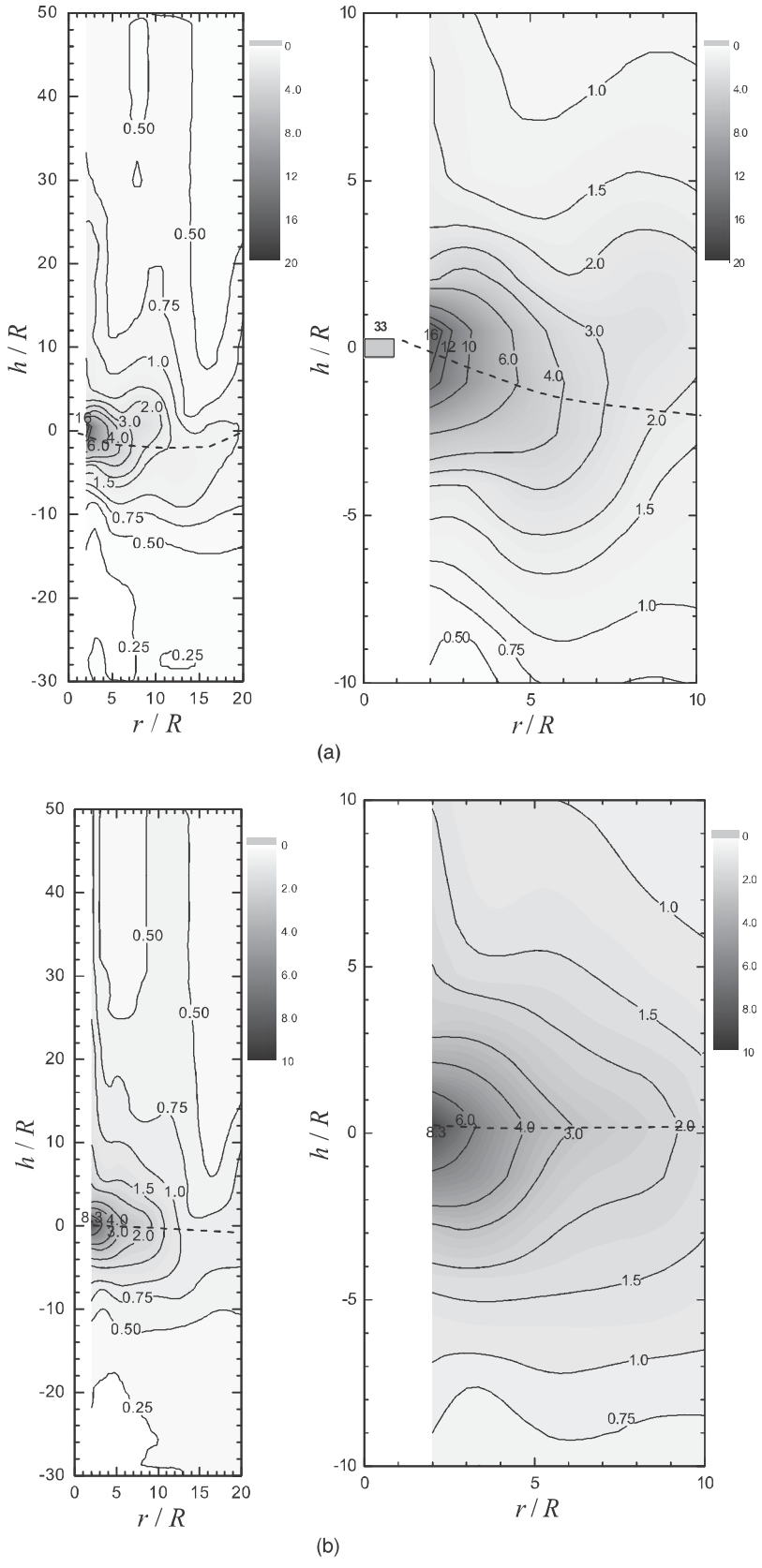


Fig. 4. Radial stress contours during installation shown at two scales: (a) moving conditions at end of each push (σ'_{rm}); (b) stationary at end of each pause (σ'_{rs}) normalized by q_c shown in percentage; dashed curves = locus connecting maxima developed in each case (Jardine et al. 2013a)

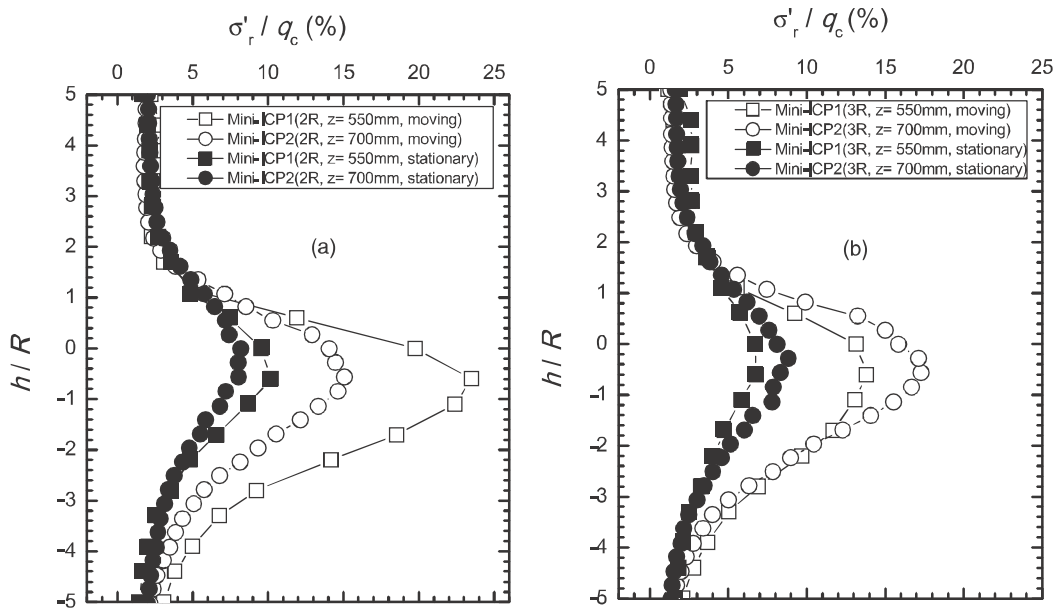


Fig. 5. Comparative moving and stationary radial stresses developed during steady penetration against relative pile tip depth h/R: (a) $r/R = 2$; (b) $r/R = 3$

varied with r/R and h/R during moving steady penetration stages while Fig. 4(b) represents the equivalent stationary pause data recorded when the pile was unloaded fully; the maximum stress loci are shown as dashed lines. The moving σ'_{rm}/q_c and stationary σ'_{rs}/q_c contours indicate intense stress concentrations emanating from the pile tip. The radial stress maximum recorded in the soil mass (at $h/R = 0.5, r/R = 2$) exceeded 16% q_c during penetration, while the zero-load stationary values were two to three times smaller. A fully active failure zone develops beneath the advancing tip where, on average, $\sigma'_{zm}/q_c = 1$ and $\sigma'_{rm} = \sigma'_{\theta m} = K_A\sigma'_{zm}$ and $K_A = \tan^2(45 + \varphi'/2) \approx 1/3$ for Fontainebleau NE34 sand at critical state under high pressures (Yang et al. 2010; Altuhafi and Jardine 2011).

Further comparisons between the moving and stationary stresses are presented in new plots given in Fig. 5 from sensors deployed in two tests at r/R ratios of 2 and 3 and depths (z) of 550 and 700 mm. Close analysis shows that the stationary and moving radial stress measurements differ most significantly near the tip ($-5 < h/R < 3$) where significant differences extend out to $r/R = 10$. Variation is mainly restricted to the $r/R < 2$ region at higher levels on the shaft. The most reliable observations of how stresses vary with r/R at set h/R values were developed from the end of installation measurements. The stationary σ'_r and σ'_θ profiles interpreted by Jardine et al. (2013a) for four h/R values are reproduced in Figs. 6(a and b). A key point to note is that the final radial stresses show maxima developing away from the shaft, between $2 < r/R < 4$ and that σ'_θ must vary steeply with r/R to maintain equilibrium giving $\sigma'_\theta > \sigma'_r$ close to the shaft. This feature is critical to understanding the marked field ageing trends of driven piles. Chow et al. (1998) and Jardine et al. (2006) proposed three possible mechanisms for the increases they observed in shaft capacity over time with piles driven in sand. One hypothesis was that shaft radial stresses increase during ageing as raised circumferential stresses relax through creep. The latter were thought to act in a sand arch formed around the displacement pile during installation, with the initially elevated hoop stresses shielding the pile shaft from higher radial stresses acting further away from the shaft. A similar mechanism was suggested independently by Åstedt et al. (1992) and was investigated in simplified cavity

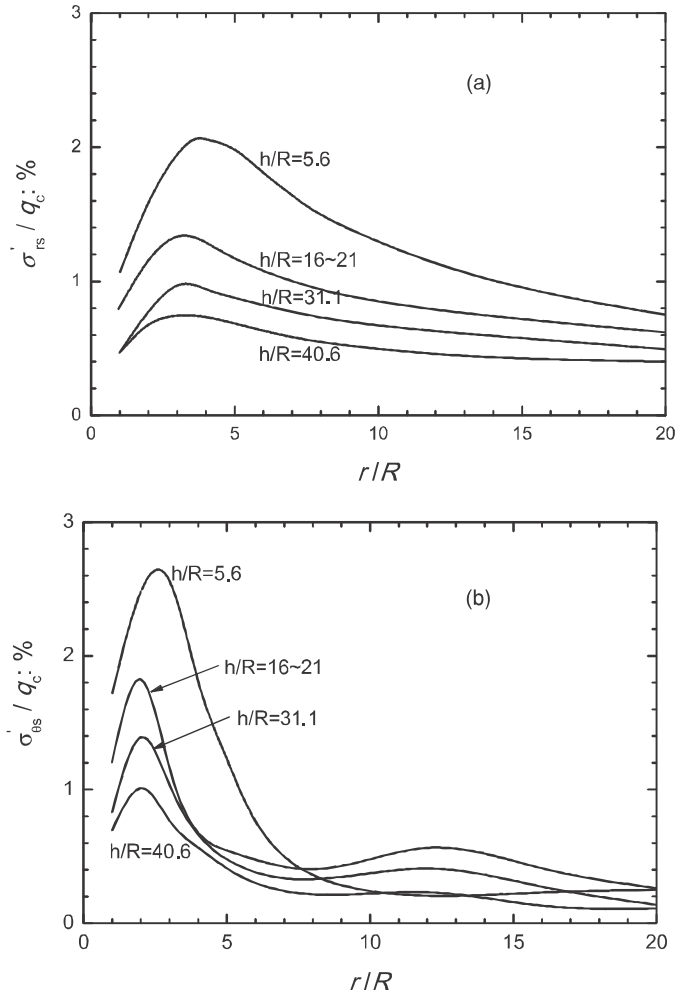


Fig. 6. Profiles interpreted for four h/R values of stationary stresses developed after final stroke of mini-ICP installation: (a) radial effective stresses; (b) circumferential effective stresses (Jardine et al. 2013a)

Downloaded from ascelibrary.org by Zhejiang University on 03/03/15. Copyright ASCE. For personal use only; all rights reserved.

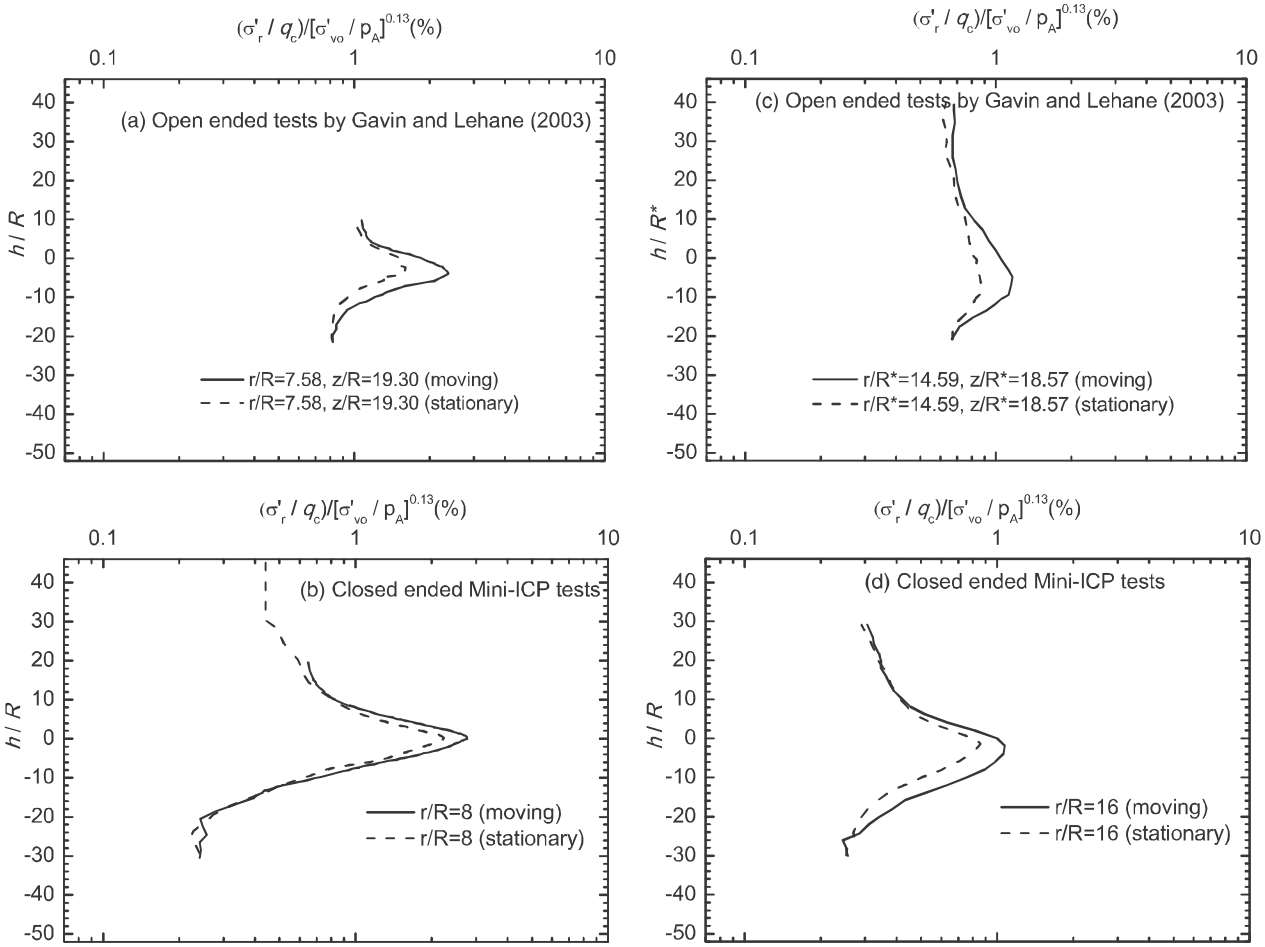


Fig. 7. Comparison of soil stresses measured in ICP and CC tests: (a) and (c) open-ended replotted (Gavin and Lehane 2003); (b) and (d) closed-ended mini-ICP

expansion/contraction analyses by White et al. (2005). The data presented in Fig. 6 present the first experimental confirmation of the supposed stress regime.

Calibration Chamber Experiments with an Open-Ended Pile

Gavin and Lehane set radial stress sensors at $r/R = 7.6$ at two depths ($z/R = 9.6$ and 19.3) around their open-ended pile. Their measurements may be compared with the mini-ICP trends after normalization, as described previously, to allow for their markedly different q_c and σ'_{zo} profiles. New comparisons are presented in Figs. 7(a–d) to show how $(\sigma'_{rm}/q_c)/(\sigma'_{zo}/p_A)^{0.13}$ varied at equivalent sand mass positions as penetration progressed. The first pair of traces considers the deeper sensor location. Noting that the open pile was tending toward plugging (with an incremental filling ratio of 38%) as it reached this depth, the open pile's outer radius is used to normalize the sensor's (h, r) coordinates in Fig. 7(a); Fig. 7(b) shows data from the equivalent $(r/R = 8)$ mini-ICP observation point. Data from the shallower of Gavin and Lehane's sensors are presented in Fig. 7(c). The pile was fully coring at this depth (IFR = 100%) so the sensor's radial distance from the center line is expressed as a multiple (14.6) of the equivalent solid pile radius R^*. The closest matching mini-ICP instrument (placed at $r/R = 16$) gave the results presented in Fig. 7(d).

Compared in this way, the two data sets show broadly similar responses, indicating that the normalized closed- and open-ended distributions are comparable, at least at the $r/R = 7.6$ positions. Greater disparity can be expected at lower r/R ratios. Both the open and closed-ended traces show marked differences between the moving and stationary stresses over the $-5 < h/R < 5$ range. They also show strong variations with h/R (or h/R^*), which are slightly steeper with the mini-ICP experiments. The mini-ICP experiments developed higher normalized radial stress maxima than Gavin and Lehane's at the deeper location, with $(\sigma'_{rm}/q_c)/(\sigma'_{zo}/p_A)^{0.13}$ rising to 2.8% rather than 2.4% seen around the partially coring open pile. This difference may be related to the partially coring (IFR = 38%) open pile condition. However, both sets show $(\sigma'_{rm}/q_c)/(\sigma'_{zo}/p_A)^{0.13}$ maxima around 1% at the shallower location when radial coordinates are matched by equating r/R for the closed mini-ICP and r/R^* for the fully coring open pile. As noted earlier, Lehane et al. (2005) preferred to account for open-ended pile conditions by reducing the q_c term in Eq. (1) as the effective pile end area ratio falls, rather than adopting R^*.

Overall, the degree of agreement is encouraging given the significant differences between the experimental arrangements. No upper surcharge or lubricated lateral boundaries were applied in Gavin and Lehane's tests. Their pile-to-chamber diameter ratio was lower and they adopted far looser sand and fewer jacking cycles. Their larger OD pile was also smoother and their stress cell calibrations less elaborate.

Downloaded from ascelibrary.org by Zhejiang University on 03/03/15. Copyright ASCE. For personal use only; all rights reserved.

Centrifuge Measurements

Allard (1990) presented traces against pile tip depth of radial stress profiles from sensors installed at $r/R = 2.67$ and six z/R ratios. As Allard did not perform centrifuge CPT testing, a q_c profile was projected from the centrifuge correlation by Gaudin et al. (2005), correcting for relative density by applying Baldi et al. (1986). Fig. 8(a) presents a reworking of Allard's stationary radial stresses, as recorded between blows applied under $50g$ acceleration and plotted here against h/R and normalized as $(\sigma'_{rs}/q_c)/(\sigma'_{zo}/p_A)^{0.13}$. Equivalent stationary mini-ICP measurements made at comparable z/R and r/R locations are shown in Fig. 8(b). The first point to recognize is the spread (among measurements made at equal r/R and h/R) of the measured stresses. The mini-ICP tests show a spread about their mean values of around $\pm 10\%$ in the stress maxima; this spread increases to around $\pm 50\%$ as h/R increases toward 30. The mini-ICP load cell calibrations also showed error bands increasing with the degree of unloading and precycling (Zhu et al. 2009). Although the centrifuge data show significantly more dispersed patterns, the averaging of multiple measurements is essential with both data sets. Despite the degree of scatter, the entirely independent experiments reveal common features, including similarly steep dependence on h/R. The centrifuge $(\sigma'_{rs}/q_c)/(\sigma'_{zo}/p_A)^{0.13}$ maxima developed at $h/R \approx 0$ falls at approximately 3.5% at $r/R = 2.67$, while the equivalent mini-ICP values average approximately 8% at $r/R = 2-3$. Several possible explanations for this significant discrepancy include

1. Errors in estimating the unmeasured centrifuge q_c-σ'_{zo} profile;
2. Limitations in the centrifuge stress-cell calibrations;
3. Installation by driving rather than cyclic jacking; and
4. The different sands, piles, shaft roughness, initial stress fields, boundary conditions, and scaling ratios.

Regarding the latter point, Allard's centrifuge bucket/pile diameter ratio was relatively low at 16, while the mini-ICP tests' chamber-to-pile ratio was 33. Allard's sensor diameter/d_{50} ratios were similar to the mini-ICP range (38 ± 12 compared with 30 ± 1), but the pile diameter, D, had lower ratios than the mini-ICP tests with respect to the sand d_{50} (95 compared with 170) and soil sensor diameters (1.9–3.7 compared with 5.5–6). Bolton et al. (1999) argue that diameter/d_{50} ratios >20 may be sufficient for centrifuge tests with smooth piles. Significant pile-sensor interference and dynamic driving densification effects might be expected in the centrifuge case, although no evidence is offered to support these speculations.

Comparisons with FEM Analyses

The key trends from the previous experiments may be compared with predictions from the three numerical analyses summarized in Table 1.

Lagrangian Multiplier FEM Analysis

Sheng et al. (2005) simulated the continuous in-flight penetration of a closed-ended pile 0.03 m in diameter with a 60° cone end into a centrifuge bucket filled with dry dense sand. Large-strain frictional contact was accommodated between the pile and soil with a reasonable interface friction angle of 27°. However, mesh dimensions beneath the tip and near the pile shaft (with element widths set between $R/4$ and $R/2$) may have limited predictive accuracy. The sand was modeled as fully drained modified cam clay (MCC), which Sheng et al. considered could simulate the drained triaxial behavior of silica sand adequately, provided a pseudo-overconsolidation ratio (OCR) is applied to ensure dilative behavior in the dry side. However, all of the experiments employed normally consolidated sand masses.

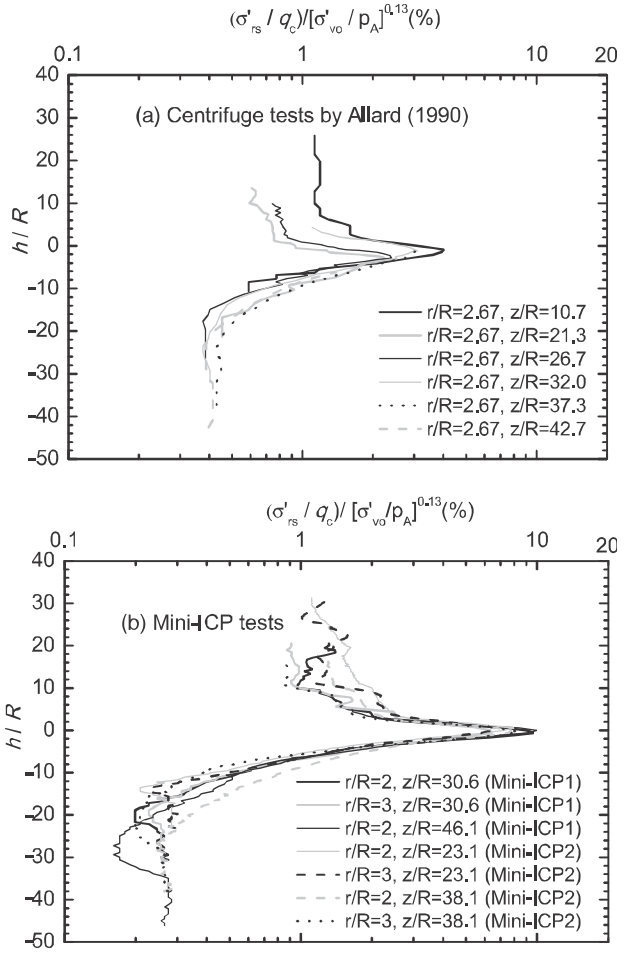


Fig. 8. Comparison of radial stresses measured in (a) centrifuge tests (Allard 1990); (b) mini-ICP tests

Sheng et al. simulated a 0.56-m-high and 0.58-m-diameter centrifuge bucket, which had a chamber/pile diameter ratio of 19.3 (compared with 33.3 in the mini-ICP tests). The sand was assumed to have $e_0 = 0.75 (D_r = 76\%)$. No surcharge was applied to the sand surface, but the initial stresses were scaled up to simulate centrifuge testing to $66.6g$ to approach prototype scale, giving $\sigma'_{zo} = 550$ kPa at the deepest point considered in Fig. 9(a). Baldi et al.'s (1986) expression was applied to estimate the q_c profile that would be expected from an idealized field CPT at prototype scale.

Examples of the stresses computed by Sheng et al. (2005) are plotted in new diagrams given in Fig. 9(a) as profiles with h/R of the moving normalized radial stresses developed at $r/R = 1.13$ for stages with tip depths $z_{tip} = 4, 8,$ and $16R$: $(\sigma'_{rm}/q_c)/(\sigma'_{zo}/p_A)^{0.13}$. The traces show the effects of the sand-mass displacement pattern evolving from one involving shallow heave toward a deep penetration mechanism. Fig. 9(b) presents the mini-ICP steady (deep) penetration moving trends observed at $r/R = 2$, which is the closest location where measurements could be made experimentally. The computed normalized maximum radial stress ratio (for deep penetration with $z/R = 16$) is 37.0%, while that interpreted by Jardine et al. (2013a) for $r/R = 1.13$ when $h/R = 0.5$ was slightly lower at 30.6%. The latter involved an interpolation between the closest measurement (of 17.8%) made at $r/R = 2$ and the $\sigma'_{rm} = K_A q_c$ maximum value applied on the conical pile tip face.

The numerical modeling and the mini-ICP tests differ in several important respects: no surface surcharge was applied in the simulation,

Downloaded from ascelibrary.org by Zhejiang University on 03/03/15. Copyright ASCE. For personal use only; all rights reserved.

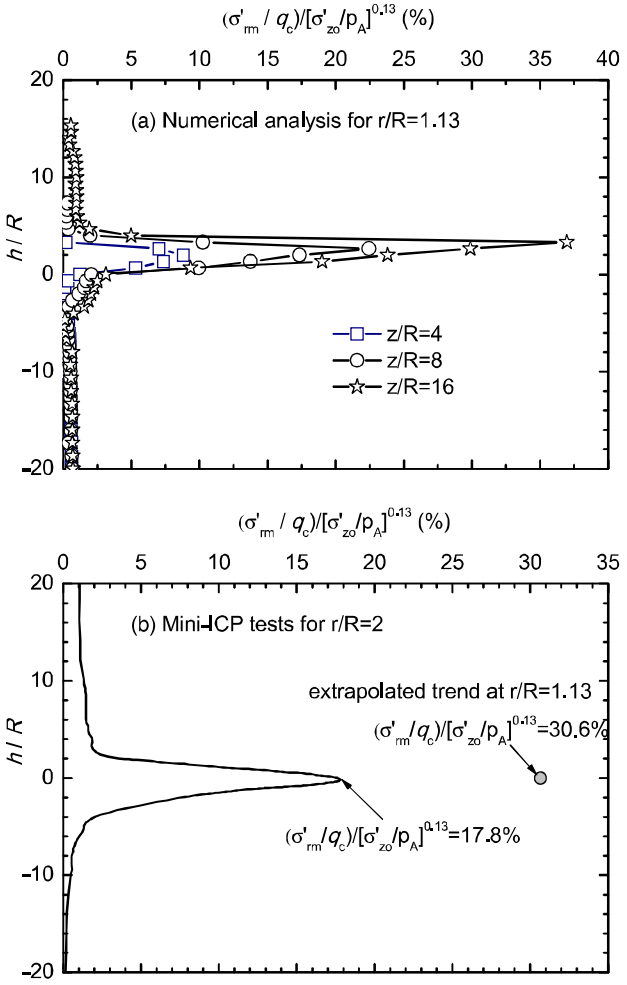


Fig. 9. Comparison of radial stresses developed during steady penetration: (a) simulated in analysis (Sheng et al. 2005); (b) measured in mini-ICP tests

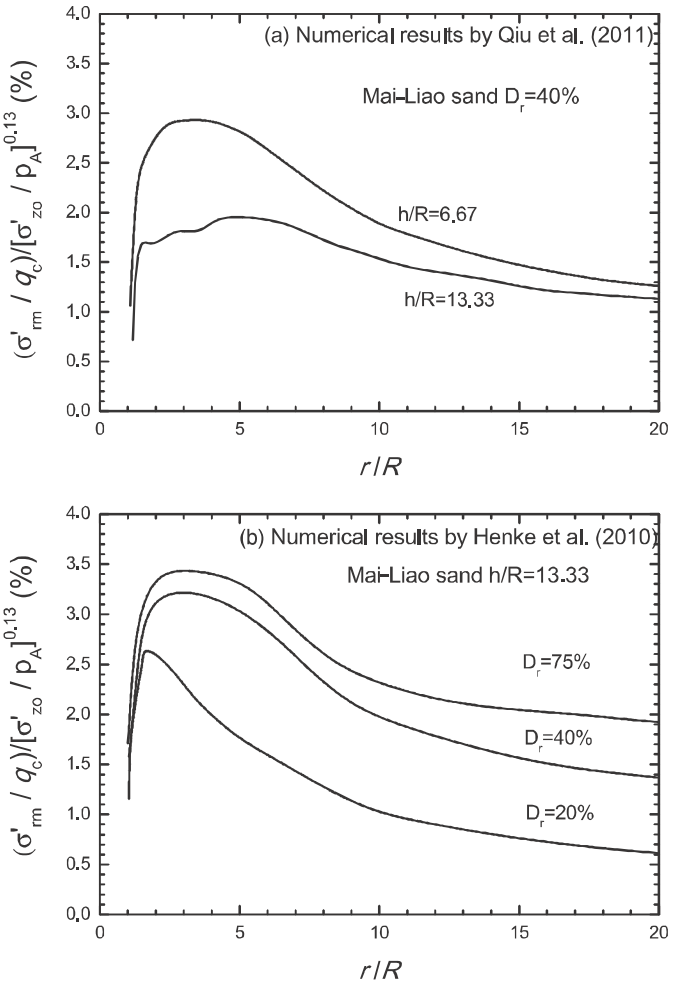


Fig. 10. Comparison between radial stresses: (a) numerical predictions made with two h/R values (Qiu et al. 2011); (b) numerical predictions made with three initial densities (Henke et al. 2010)

nor was any attempt made to match the cyclic jacking/driving process, or the interface shear phenomena of finite dilation, banding, or particle crushing. The q_c profile is also uncertain. However, Sheng et al.'s (2005) analysis illustrates how the normalized stresses evolve with penetration. Their normalized deep penetration profile provides a good first principles prediction of the observed steep variations with h/R that are due purely (under monotonic penetration) to the system geometry, as well as predicting stress maxima that agree reasonably with the experimental trend.

CEL FEM Analyses

Analyses employing a CEL technique applied to a 300-mm diameter closed conically tipped pile penetrating monotonically in dry sand to a 5-m depth are reported by Henke et al. (2010) and Qiu et al. (2011). The soil was assumed to match uniform beds of Taiwanese Mai-Liao sand (Henke 2008) and a hypoplasticity constitutive law (Herle 1997) applied. Simulations were made for sand with relative densities between 20 and 75% and Coulomb pile-sand interface friction was adopted assuming $\delta' = \varphi'/3$, although higher angles could be expected from practical interface shear tests (Ho et al. 2011). CPT q_c profiles were estimated for comparison from Baldi et al. (1986).

The variations in the moving sand radial stresses were reported separately by Henke et al. (2010) and Qiu et al. (2011) for radial profiles located at two depths extending out to 5 m. Figs. 10(a and b) show the results for three relative densities reprocessed for this article as $(\sigma'_{rm}/q_c)/(\sigma'_{zo}/p_A)^{0.13}$ ratios plotted against r/R, considering horizontal profiles set at $h/R = 6.67$ and 13.33. Comparison with the mini-ICP experiments is best made with the stationary profiles presented earlier in Fig. 6(a). It can be recalled that the stationary and moving radial stress measurements differ most significantly at h/R ratios between ± 3 and close to the shaft ($r/R < 2$), so comparisons with the moving numerical analysis profiles given in Figs. (10a and b) are legitimate except, potentially, in the near-field $r/R < 2$ region.

As with Sheng et al.'s (2005) analysis, significant differences exist between the numerical model and the mini-ICP tests. These include the 50–200 full load-unload cycles imposed in the mini-ICP's installation, the perfectly uniform soils and unsurcharged sands simulated in the FE analysis, as well as the interface shear and particle breakage processes. The soil model may not have been able to fully match the nonlinear, inelastic, and anisotropic behavior of real sands, including their stress-history–dependent shear strength, stiffness, dilatancy, and void ratio characteristics. Despite these potential reservations, the numerical analyses capture a similar dependence of the sand stress regime on the geometrical (h/R and r/R) and sand state (q_c and σ'_{zo}) variables. The reprocessed numerical results show a clear decay in stresses with increasing h/R in

Downloaded from ascelibrary.org by Zhejiang University on 03/03/15. Copyright ASCE. For personal use only; all rights reserved.

the predictions for $D_r = 40\%$ [Fig. 10(a)], and also comparable radial distributions to the experiments in Fig. 10(b), including maxima developing away from the shaft at $2 < r/R < 4$. Jardine et al. (2013a) show that the radial stress maxima seen in the $2 < r/R < 4$ range in Figs. 5 and 10 necessarily imply steeply varying σ'_θ stress components with $\sigma'_\theta > \sigma'_r$ in the near field surrounding the pile shaft. The profile of radial stress with r/R (defined at $h/R = 13.33$) shows (for the most comparable $D_r = 75\%$ case) a maximum in $(\sigma'_{rm}/q_c)/(\sigma'_{zo}/p_A)^{0.13} \approx 2.5\%$ that exceeds the midpoint of the stationary experimental range (1.3–2% for h/R values between 5.6 and ≈20) by about 50%. Such quantitative discrepancies might be reduced in analyses that accounted for the installation of load-cycling or grain-crushing beneath the advancing tip (or in the shaft interface shear zone).

Finite-Element Analysis Incorporating Grain Crushing

Zhang et al. (2013) adopted an arbitrary Lagrangian Eulerian (ALE) FE approach with remeshing and variable remapping to simulate monotonic penetration. Their breakage mechanics model provided good predictions for the evolving grain-size distributions (GSD) trends and their tip resistance predictions matched the experiments well (see Fig. 2). One feature that was not captured analytically was the observed thickening of the interface shear band with increasing h/R that Yang et al. (2010) related to interface abrasion and cyclic installation effects.

A discussion with Einav (I. Einav, personal communication, 2012) led to further processing of Zhang et al.'s simulations. Previously unpublished profiles of predictions for the moving radial and circumferential effective stresses developed during the pile installation were communicated to the writers and reprocessed to give the normalized profiles of stresses varying with r/R at three h/R levels in Figs. 11(a and b). These traces may be compared with the equivalent stationary profiles interpreted from the mini-ICP experiments given in Fig. 5. While the experimental and analytical profiles do not cover exactly the same h/R values (and should not be compared directly at $r/R < 2$) they show many similarities. As with the analyses of Henke et al. (2010) and Qiu et al. (2011), radial stress maxima are predicted, although these develop slightly further away from the shaft ($3 < r/R < 8$). The computed σ'_θ profiles show the steep radial variations and the $\sigma'_\theta > \sigma'_r$ trend, as interpreted by Jardine et al. (2013a), close to the shaft. As expected, the radial stress profiles fall as h/R increases, although the variation at higher h/R values appears relatively minor. The maximum value of $(\sigma'_{rm}/q_c)/(\sigma'_{zo}/p_A)^{0.13}$ predicted at $h/R = 6$ is 2.1%, which falls close to that observed experimentally (2%) at $h/R = 5.6$.

Further agreement between the predicted and measured near tip stress regimes is illustrated in three new normalized comparison plots in Fig. 12 that consider how the radial, circumferential, and vertical effective stress profiles vary with r/R at h/R values of 0 and 0.5.

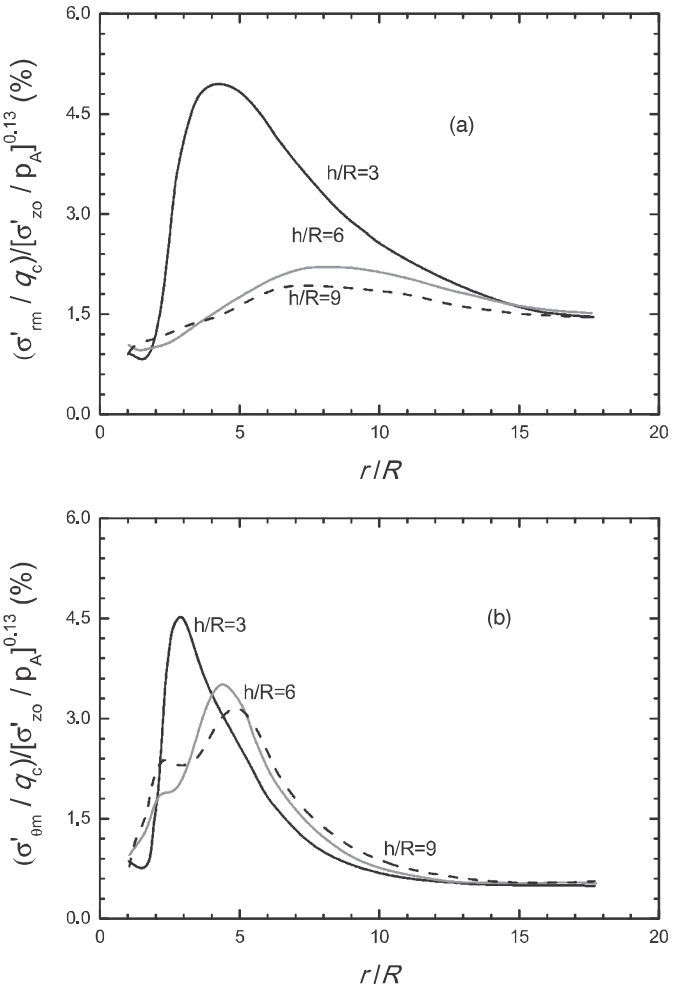


Fig. 11. Normalized stresses developed at various h/R positions from numerical simulations (I. Einav, personal communication, 2012): (a) radial; (b) circumferential

Summary and Conclusions

This paper has explored the cylindrical normal stresses developed around piles penetrating into normally consolidated silica sands, drawing together a trio of independent experimental investigations and three numerical analyses. The interpretation has synthesized measurements and predictions made at points with initial effective stresses ranging from 10 to 550 kPa and states from loose-to-dense by

1. Normalizing stresses with respect to local CPT q_c and a nondimensional vertical stress ratio $(\sigma'_{zo}/p_A)^{0.13}$; and
2. Adopting the tip as the origin for nondimensional spatial coordinates $(h/R,\ r/R)$ for closed-ended conditions and $(h/R^*,\ r/R^*)$ for the stresses developed at moderate radial distances around open-ended piles.

The great care required to make reliable stress measurements has been emphasized. Experiments may be subject to a wide range of potential imperfections and sources of scatter or error. Equally, numerical modeling of the installation process poses a series of significant challenges. Despite these difficulties, quantification of the stress conditions developed around displacement piles in sand appears to becoming feasible. The following clear trends are evident:

1. Deep penetration radial stress measurements and predictions, obtained by a wide range of approaches, show broadly similar strong dependence on relative pile tip depth, h/R, irrespective of the sand relative density and pile installation method (discontinuous jacking, driving, or continuous pushing). Further studies are required to establish the detailed effects of the number of installation cycles and test boundary conditions.
2. Use of the equivalent pile radius, R^*, proposed by Jardine et al. (2005), allows the stresses developed around coring open piles to be reconciled with those developed with closed ends. Similar normalized stress ratios were developed in measurements made at $r/R = 7.6$ at comparable normalized

Downloaded from ascelibrary.org by Zhejiang University on 03/03/15. Copyright ASCE. For personal use only; all rights reserved.

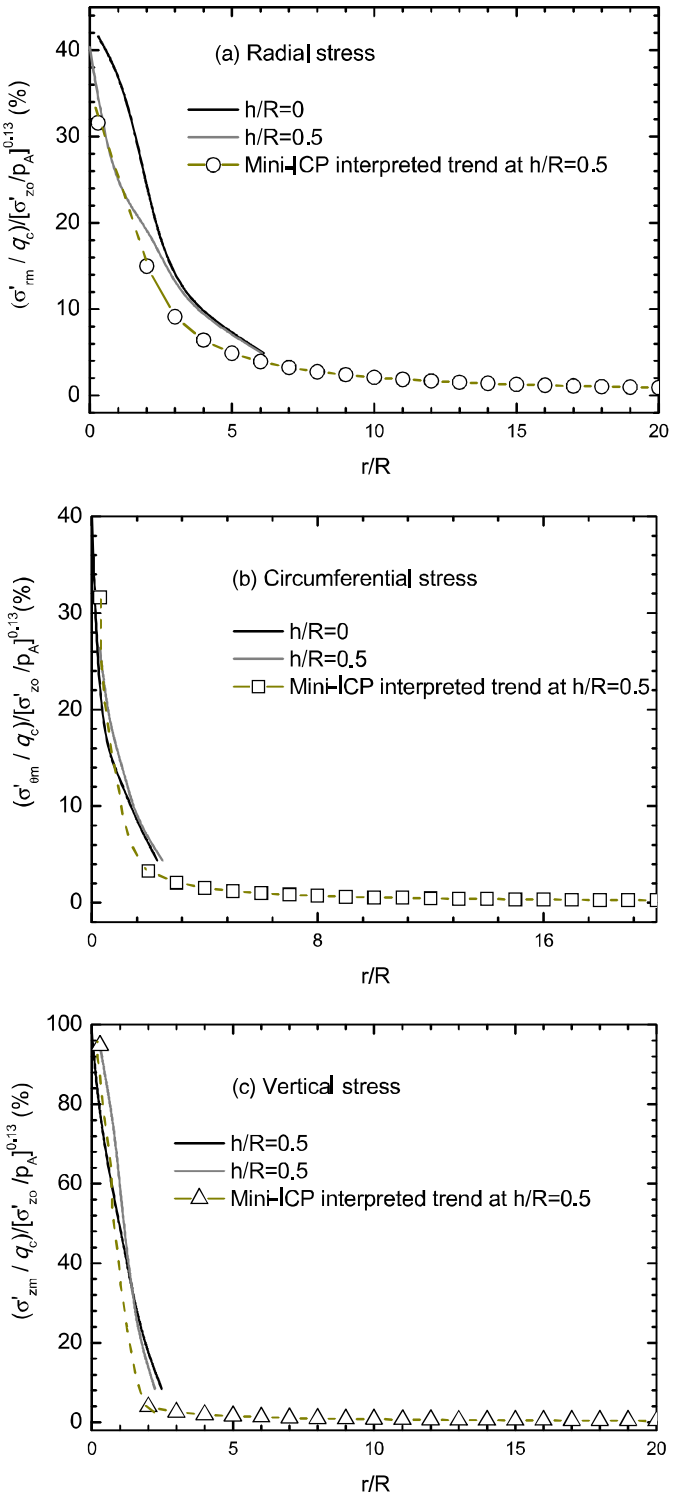


Fig. 12. Stress profiles established experimentally and analytically close to pile cone tip during penetration: (a) radial; (b) circumferential; (c) vertical

positions, although greater variations are expected closer to the pile shaft.

3. The normalized radial stress maxima defined during the steady penetration stages of both experiments and numerical analyses generally conform to within ±50% of the equivalent measurements made at the same normalized locations in the benchmark mini-ICP experiments. Possible explanations have been suggested for any significant discrepancies identified between the disparate data sets.
4. Monotonic numerical analyses and cyclically advanced experiments both indicate that radial stress maxima develop away from the shaft in the $2 < r/R < 8$ range, leading to σ'_θ necessarily varying steeply with the radius, and $\sigma'_\theta > \sigma'_r$ conditions applying close to the shaft.

Scope exists for closer analysis by investigating further factors such as the performance of soil stress sensors, scale effects relating to the relative diameters of the piles with respect to the grain, and test chamber and soil-stress sensor diameters. Further studies to establish centrifuge CPT profiles and consider the effects of different installation styles would also be beneficial, as would further investigations of the effects of pile tip geometry and installation procedure, as well as prior overconsolidation of the sand mass. The incorporation of particle breakage into numerical simulations leads to interesting results. Further elaboration that allows for installation cycles, interface shear, sand anisotropy, and other parameters to be considered with greater representation appears warranted.

Acknowledgments

The research herein was funded by Natural Science Foundation of China (Nos. 51178421, 51322809, and 51078329), the U.K. Royal Society, the Chinese Ministry of Education Distinguished Overseas Professorship Program, Shell U.K. Limited, the U.K. Health and Safety Executive, the U.K. Engineering Physical Sciences Research Council, and Total, France. Their support is gratefully acknowledged as are the contributions made to the mini-ICP experiments by colleagues at INPG Grenoble and Imperial College including: Professor Pierre Foray, Dr. Mark Emerson, Dr. Cristina Tsuha, Mr. Jean-Benoit Toni, Mr. Steve Ackerley, Mr. Clive Dalton, Mr. Bernard Rey, Mr. Alan Bolsher, Mr. Matias Silva, and Mr. Francesco La Malfa. Assistance from Professor Itai Einav in sharing his team's numerical analysis results is also acknowledged with thanks.

Notation

The following symbols are used in this paper:

D = diameter; $D_{chamber}$ and D_{pile} are calibration chamber and pile diameters, respectively;
D_r = relative density of sand;
d_{50} = particle diameter that 50% of all particles are finer(smaller) by weight;
e_0 = initial void ratio;
h = height above pile tip (positive) or depth below pile tip (negative);
K_A = Rankine coefficients of active earth pressure;
L_p = pile penetration depth;
p_A = atmospheric pressure;
q_c = CPT cone resistance;
R = pile radius;
R_i = inner radius of an open-ended pile;
R_0 = outer radius of an open-ended pile;
R^* = equivalent radius of an open-ended pile;
r = radius of point from pile axis;
z = depth below the sand surface;
z_{tip} = depth of pile tip below the sand surface;
δ' = effective angle of interface shearing resistance;

Downloaded from ascelibrary.org by Zhejiang University on 03/03/15. Copyright ASCE. For personal use only; all rights reserved.

σ'_r = effective radial stress; σ'_{rm}, σ'_{rs}, $\sigma'_{r\max}$ are moving, stationary, and maximum values;
σ'_{rc} = equalized radial effective stress;
σ'_z = effective vertical stress; σ'_{zm}, σ'_{zs}, $\sigma'_{z\max}$ are moving, stationary, and maximum values; σ'_{z0} is free-field vertical effective stress;
σ'_θ = effective circumferential stress; $\sigma'_{\theta m}$, $\sigma'_{\theta s}$, $\sigma'_{\theta\max}$ are moving, stationary, and maximum values;
σ'_1, σ'_2, σ'_3 = major, intermediate, and minor principal effective stresses;
τ_{rzf} = local shaft resistance of piles; and
φ' = effective angle of shearing resistance, φ'_{cs} is a critical state value.

References

Allard, M. A. (1990). "Soil stress field around driven piles." Ph.D. thesis, California Institute of Technology, Pasadena, CA.

Altuhafi, F., and Jardine, R. J. (2011). "Effect of particle breakage and strain path reversal on the properties of sands located near to driven piles." *Deformation characteristics of geomaterials*, Vol. 1, IOS-Press, Hanrimwon, Seoul, 386–395.

American Petroleum Institute (API). (2011). *ANSI/API recommended practice 2GEO*, 1st Ed., *RP2GEO*, Washington, DC.

Arroyo, M., Butlanska, J., Gens, A., Calvetti, F., and Jamiolkowski, M. (2011). "Cone penetration tests in a virtual calibration chamber." *Geotechnique*, 61(6), 525–531.

Åstedt, B., Weiner, L., and Holm, G. (1992). "Increase in bearing capacity with time for friction piles in silt and sand." *Proc., Nordic Geotechnical Meeting*, 411–416.

Baldi, G., Bellotti, R., Ghionna, V., Jamiolkowski, M., and Pasqualini, E. (1986). "Interpretations of CPT's and CPTU's, 2nd part: Drained penetration of sands." *Proc., 4th Int. Conf. on Field Instrumentation and In-situ Measurements*, Nanyang Technological Institute, Singapore, 143–156.

Bolton, M. D., et al. (1999). "Centrifuge cone penetration tests in sand." *Geotechnique*, 49(4), 543–552.

Campos, J. L. E., Vargas, E. A., Bernardes, G., Ibañez, J. P., and Velloso, R. Q. (2005). "Numerical experiments with discrete elements to simulate pile penetration in granular soils." *Proc., XXVI Iberian Latin-American Congress on Computational Methods in Engineering*, Brazilian Association for Comp. Mechanics (ABMEC) and Latin American Association of Comp. Methods in Engineering (AMC), Guarapari, Espírito Santo, Brazil.

Chow, F. C. (1997). "Investigations into displacement pile behaviour for offshore foundations." Ph.D. thesis, Imperial College London, London.

Chow, F. C., Jardine, R. J., Brucy, F., and Nauroy, J. F. (1998). "The effects of time on the capacity of pipe piles in dense marine sand." *J. Geotech. Geoenviron. Eng.*, 10.1061/(ASCE)1090-0241(1998)124:3(254), 254–264.

Clausen, C. J. F., Aas, P. M., and Karlsrud, K. (2005). "Bearing capacity of driven piles in sand, the NGI approach." *Frontiers in offshore geotechnics*, S. Gourvenec and M. Cassidy, eds., Taylor & Francis, London, 677–683.

de Nicola, A., and Randolph, M. F. (1997). "Plugging behaviour of driven and jacked piles in sand." *Geotechnique*, 47(4), 841–856.

Doherty, P., and Gavin, K. (2010). "A statistical review of CPT data and the implications for pile design." *Proc., 2nd Int. Symp. on Cone Penetration Testing (CPT10)*, P. Mayne, ed., CPT'10 Organizing Committee.

Feng, T. W., Chen, K. H., Su, Y. T., and Shi, Y. C. (2000). "Laboratory investigation of efficiency of conical-based pounders for dynamic compaction." *Geotechnique*, 50(6), 667–674.

Foray, P. (1991). "Scale and boundary effects on calibration chamber pile tests." *Proc., 1st Int. Conf. on Calibration Chamber Testing*, Clarkson Univ., Postdam, NY.

Foray, P., Balachowski, L., and Colliat, J.-L. (1998). "Bearing capacity of model piles driven into dense overconsolidated sands." *Can. Geotech. J.*, 35(2), 374–385.

Foray, P., Colliat, J.-L., and Nauroy, J. F. (1993). "Bearing capacity of driven model piles in dense sands from calibration chamber tests." *Proc., 25th Offshore Technology Conf.*, Offshore Technology Conference, Houston.

Gaudin, C., Schnaid, F., and Garnier, J. (2005). "Sand characterization by combined centrifuge and laboratory tests." *Int. J. Phys. Model. Geotech.*, 5(1), 42–56.

Gavin, K. G., and Lehane, B. M. (2003). "The shaft capacity of pipe piles in sand." *Can. Geotech. J.*, 40(1), 36–45.

Golightly, C. R., and Nauroy, J.-F. (1990). "End bearing capacity of piles in calcareous sands." *Proc., Offshore Technology 22nd Annual Conf.*, Offshore Technology Conference, Houston.

Grabe, J., and Henke, S. (2010). "High-performance finite element and coupled Eulerian-Lagrangian simulations of pile installation processes." *Proc., 4th Int. Conf. Structural Engineering, Mechanics and Computation*, CRC Press, Boca Raton, FL.

Henke, S. (2008). "Herstellungseinflüsse aus Pfahlrammung im Kaimauerbau." Ph.D. thesis, Veröfentlichungen des Instituts für Geotechnik und Baubetrieb der TU, Hamburg-Harburg, Germany.

Henke, S., and Grabe, J. (2006). "Simulation of pile driving by 3-dimensional finite-element analysis." *Proc., 17th European Young Geotechnical Engineers' Conf.*, V. Szavits-Nossan, ed., Croatian Geotechnical Society, Zagreb, Croatia.

Henke, S., and Grabe, J. (2007). "Simulation of pile installation by three-dimensional finite element analyses." *Darmstadt Geotechnics*, 15, 179–192.

Henke, S., Qiu, G., and Grabe, J. (2010). "A coupled Eulerian Lagrangian approach to solve geotechnical problems involving large deformations." *Proc., 7th European Conf. on Numerical Methods in Geotechnical Engineering (NUMGE)*, CRC Press, Boca Raton, FL.

Herle, I. (1997). "Hypoplastizität und Granulometrieeinfacher Korngerüste." Ph.D. thesis. Institut für Bodenmechanik und Felsmechanik der Universität Karlsruhe, Karlsruhe, Germany.

Ho, T. Y. K., Jardine, R. J., and Minh, N. A. (2011). "Large displacement interface shear between steel and granular media." *Geotechnique*, 61(3), 221–234.

Huang, A. B., and Hsu, H. H. (2005). "Cone penetration tests under simulated field conditions." *Geotechnique*, 55(5), 345–354.

Jardine, R. J., and Chow, F. C. (2007). "Some developments in the design of offshore piles." *Proc., 6th Int. Conf. on Offshore Site Investigations and Geotechnics*, Society for Underwater Technology, London.

Jardine, R. J., Chow, F. C., and Overy, R. (2005). *ICP design methods for driven piles in sands and clays*, Thomas Telford, London.

Jardine, R. J., Standing, J. R., and Chow, F. C. (2006). "Some observations of the effects of time on the capacity of piles driven in sand." *Geotechnique*, 56(4), 227–244.

Jardine, R. J., Zhu, B. T., Foray, P., and Dalton, J. C. P. (2009). "Experimental arrangements for the measurements of soil stresses around a displacement pile." *Soils Found.*, 49(5), 661–673.

Jardine, R. J., Zhu, B. T., Foray, P., and Yang, Z. X. (2013a). "Interpretation of stress measurements around closed-ended displacement piles in sand." *Geotechnique*, 63(8), 613–627.

Jardine, R. J., Zhu, B. T., Foray, P., and Yang, Z. X. (2013b). "Measurement of stresses around closed-ended displacement piles in sand." *Geotechnique*, 63(1), 1–17.

Kinloch, H., and O'Sullivan, C. (2007). "A micro-mechanical study of the influence of penetrometer geometry on failure mechanisms in granular soils." *Geo-Denver Conf., Advances in Measurement and Modeling of Soil Behavior*, ASCE, Reston, VA.

Klotz, E. U., and Coop, M. R. (2001). "An investigation of the effect of soil state on the capacity of driven piles in sands." *Geotechnique*, 51(9), 733–751.

Knudsen, S., Langford, T., Lacasse, S., and Aas, P. M. (2012). "Axial capacity of offshore piles driven in sand using four CPT-based methods." *Proc., 7th Int. Conf. on Offshore Site Investigations and Geotechnics*, Society for Underwater Technology, London.

Kolk, H. J., Baaijens, A. E., and Senders, M. (2005). Design criteria for piles in silica sands. *Frontiers in offshore geotechnics*, S. Gourvenec and M. Cassidy, eds., Taylor & Francis, London, 711–716.

Lau, Y., Ooi, G., and Wang, Y. (2010). "Three-dimensional DEM simulations on pile installation." *Geomechanics and geotechnics: From micro to macro*, M. Jiang et al., eds., CRC Press, Boca Raton, FL, 579–583.

Downloaded from ascelibrary.org by Zhejiang University on 03/03/15. Copyright ASCE. For personal use only; all rights reserved.

Lehane, B. M., Jardine, R. J., Bond, A. J., and Frank, R. (1993). "Mechanisms of shaft friction in sand from instrumented pile tests." *J. Geotech. Engrg.*, 10.1061/(ASCE)0733-9410(1993)119:1(19), 19–35.

Lehane, B. M., Schneider, J. A., and Xu, X. (2005). "CPT based design of driven piles in sand for offshore structures." *Rep. GEO 05345*, Univ. of Western Australia, Perth, WA, Australia.

Levacher, D., Morice, Y., Favraud, C., and Thorel, L. (2008). "A review of pile drivers for testing in centrifuge." *10th National Coastal Engineering—Civil Engineering, Instrumentation, Measurement, Imaging and Remote Sensing Conf.*, Xèmes Journées Nationales Génie Côtier – Génie Civil, Sophia Antipolis, France.

Nauroy, J. F., and Le Tirant, P. (1983). "Model tests of piles in calcareous sands." *Proc., Conf., on Geotechnical Practice in Offshore Engineering*, Geo-Institute, Univ. of Texas at Austin, Austin, TX, 356–369.

Overy, R. (2007). "The use of ICP design methods for the foundations of nine platforms installed in the U.K. North Sea." *Proc., 6th Int. Conf. on Offshore Site Investigations and Geotechnics*, Society for Underwater Technology, London.

Paik, K., Lee, J., and Kim, D. (2011). "Axial response and bearing capacity of tapered piles in sandy soil." *J. ASTM Geotech Test.*, 34(2), 122–130.

Paik, K., and Salgado, R. (2003). "Determination of bearing capacity of open-ended piles in sand." *J. Geotech. Geoenviron. Eng.*, 10.1061/(ASCE)1090-0241(2003)129:1(46), 46–57.

Qiu, G., Henke, S., and Grabe, J. (2011). "Application of a coupled Eulerian-Lagrangian approach on geomechanical problems involving large deformations." *Comput. Geotech.*, 38(1), 30–39.

Rimoy, S. P. (2013). "Ageing and axial cyclic loading studies of displacement piles in sands." Ph.D. thesis, Imperial College, London.

Sakr, M., and Naggar, M. (2003). "Centrifuge modeling of tapered piles in sand." *J. ASTM Geotech Test.*, 26(1), 1–13.

Salgado, R., Mitchell, J. K., and Jamiolkowski, M. (1998). "Calibration chamber size effects on penetration resistance in sand." *J. Geotech. Geoenviron. Eng.*, 10.1061/(ASCE)1090-0241(1998)124:9(878), 878–888.

Sheng, D., Dieter Eigenbrod, K., and Wriggers, P. (2005). "Finite element analysis of pile installation using large-slip frictional contact." *Comput. Geotech.*, 32(1), 17–26.

White, D. J., and Bolton, M. D. (2004). "Displacement and strain paths during plane-strain model pile installation in sand." *Géotechnique*, 54(6), 375–397.

White, D. J., and Lehane, B. M. (2004). "Friction fatigue on displacement piles in sand." *Géotechnique*, 54(10), 645–658.

White, D. J., Schneider, J. A., and Lehane, B. M. (2005). "The influence of effective area ratio on shaft friction of displacement piles in sand." *Frontiers in offshore geotechnics*, S. Gourvenec and M. Cassidy, eds., Taylor & Francis, London, 741–749.

Yang, Z. X., Jardine, R. J., Zhu, B. T., Foray, P., and Tsuha, C. H. C. (2010). "Sand grain crushing and interface shearing during displacement pile installation in sand." *Geotechnique*, 60(6), 469–482.

Zhang, C., Nguyen, G. D., and Einav, I. (2013). "The end-bearing capacity of piles penetrating into crushable soils." *Geotechnique*, 63(5), 341–354.

Zhu, B. T., Jardine, R. J., and Foray, P. (2009). "The use of miniature soil stress measuring sensors in applications involving stress reversals." *Soils Found.*, 49(5), 675–688.

Downloaded from ascelibrary.org by Zhejiang University on 03/03/15. Copyright ASCE. For personal use only; all rights reserved.